

This is the accepted manuscript made available via CHORUS. The article has been published as:

## Nanoscale Electron Bunching in Laser-Triggered Ionization Injection in Plasma Accelerators

X. L. Xu, C.-H. Pai, C. J. Zhang, F. Li, Y. Wan, Y. P. Wu, J. F. Hua, W. Lu, W. An, P. Yu, C. Joshi, and W. B. Mori

Phys. Rev. Lett. **117**, 034801 — Published 15 July 2016

DOI: [10.1103/PhysRevLett.117.034801](https://doi.org/10.1103/PhysRevLett.117.034801)

# Nano-scale electron bunching in laser-triggered ionization injection in plasma accelerators

X. L. Xu,<sup>1</sup> C. J. Zhang,<sup>2</sup> F. Li,<sup>2</sup> Y. Wan,<sup>2</sup> Y. P. Wu,<sup>2</sup> J. F. Hua,<sup>2</sup>  
C.-H. Pai,<sup>2</sup> W. Lu,<sup>2,3,\*</sup> W. An,<sup>1</sup> P. Yu,<sup>1</sup> C. Joshi,<sup>1</sup> and W. B. Mori<sup>1</sup>

<sup>1</sup>*University of California, Los Angeles, California 90095, USA*

<sup>2</sup>*Department of Engineering Physics, Tsinghua University, Beijing 100084, China*

<sup>3</sup>*IFSA Collaborative Innovation Center, Shanghai Jiao Tong University, Shanghai 200240, China*

(Dated: July 7, 2016)

Ionization injection is attractive as a controllable injection scheme for generating high quality electron beams using plasma-based wakefield acceleration. Due to the phase dependent tunneling ionization rate and the trapping dynamics within a nonlinear wake, the discrete injection of electrons within the wake is nonlinearly mapped to discrete final phase space structure of the beam at the location where the electrons are trapped. This phenomenon is theoretically analyzed and examined by three-dimensional particle-in-cell simulations which show that three dimensional effects limit the wave number of the modulation to between  $> 2k_0$  and about  $5k_0$ , where  $k_0$  is the wavenumber of the injection laser. Such a nano-scale bunched beam can be diagnosed by and used to generate coherent transition radiation and may find use in generating high-power ultraviolet radiation upon passage through a resonant undulator.

Due to the ability to sustain ultra-high acceleration gradients (GV/cm), the field of plasma-based wakefield acceleration has attracted much attention in the past two decades [1]. Recently, ionization injection has been proposed and demonstrated [2–9] as a viable injection scheme and investigated for generating high brightness ( $\sim 10^{19}$  A/rad<sup>2</sup>/m<sup>2</sup>), stable, and tunable electron beams [10–15]. The basic idea is that the trapping threshold of an electron is reduced when it is born inside the wake-field near the maximum of wake’s potential compared to an electron from a pre-ionized plasma. Such high brightness beams are needed for future free-electron-laser and collider applications.

The key to generating a high brightness beam is to limit the volume within the wake where injection of electrons occurs [16]. In the case where injection is from field ionization due to a laser pulse, the ionization volume is limited by choosing the intensity of the injection pulse(s) close the ionization threshold of bound electrons. Therefore, electrons are mostly born near the peaks and the troughs of the oscillating laser electric field. The phase-dependent ionization leads to an intrinsic initial phase space discretization at twice the optical frequency, which is known to produce third harmonic generation in tunnel ionized plasma [17, 18].

We show in this Letter using theory and fully three-dimensional (3D) particle-in-cell (PIC) simulations, that when ionization occurs on either side of the peak of the wake potential the electron bunch can be strongly modulated in space on the nanometer scale when it becomes trapped. In the 1D limit the spacing of the modulations can be made arbitrarily small. However, we show that 3D effects limit the discretization pattern to less than one-fifth the laser wavelength. In previous work, the generation of distinct energy peaks within a single bunch were described from ionization in different optical cycles [19]

or from ionization at distinct propagation times [20]. On the other hand, here we show that ionization injection within each optical phase of the laser at one propagation distance can lead to the formation of distinct current peaks. Such an ultra-short and nano-bunched electron beam can be diagnosed by and used to generate coherent transition radiation (CTR) [21], could generate a train of atto-second X-ray pulses through betatron radiation in the plasma wake, and be used to produce high power coherent EUV radiation in a short resonant undulator.

To illustrate the concept, we first consider ionization injection using a single laser pulse as shown in Fig. 1(a). An 800nm laser pulse polarized in the  $x$  direction with normalized vector potential  $a_0 = 2$ ,  $w_0 = 14\mu\text{m}$  and a pulse length (fwhm of energy) of 26fs, propagates into a mixture of pre-ionized plasma ( $n_p = 2 \times 10^{18} \text{ cm}^{-3}$ ) and  $\text{N}^{5+}$  ions. The pre-ionized electrons form a non-linear wake. As has been observed previously [4], the K-shell electrons of nitrogen with high ionization potentials (IPs) are released during the rising edge of the wake potential [Fig. 1(a)], then slip to the back of the wake where some of these electrons are trapped [4]. This process is examined using the 3D PIC code OSIRIS [22] using a moving window [23]. We define the  $z$  axis to be the laser propagating direction. The code uses the Ammosov-Delone-Krainov (ADK) tunneling ionization model [24]. The IPs of the sixth and seventh nitrogen electrons are  $I_p \approx 552.1\text{eV}, 667.0\text{eV}$  respectively, and the Keldysh parameter in this simulation is  $\gamma_K = \sqrt{I_p}/2U_p \approx 0.023, 0.021 \ll 1$ ; therefore the ADK model should be valid. The simulation window has a dimension of  $63.5 \times 63.5 \times 38.1\mu\text{m}$  with  $500 \times 500 \times 1500$  cells in the  $x, y$  and  $z$  directions, respectively.

The  $(\xi_i, x_i)$  space distribution of the trapped electrons when they are ionized is shown in Fig. 1(b), where  $\xi \equiv v_\phi t - z$  is the relative longitudinal position and  $v_\phi$  is

the phase velocity of the wake. Due to the laser phase-dependent ionization probability, the initial electron distribution has a strong modulation at  $2k_0$ , where  $k_0$  is the wavenumber of the laser pulse. After being released, the electrons slip to the back of the wake and are accelerated by the longitudinal electric field in the wake. Under the quasi-static approximation,  $\gamma - (v_\phi/c)p_z - \psi = \text{Const}$  [25], where  $\psi \equiv (e/mc^2)[\phi - (v_\phi/c)A_z]$  is the pseudo potential,  $\psi$  in the fully blown-out wake can be expressed as  $\psi \approx [r_b^2(\xi) - r^2]/4$  [26][27]. Here  $r_b(\xi)$  is the normalized radius of the ion channel that has a spherical shape for a sufficiently large maximum blowout radius  $r_m$  given by  $r_b^2(\xi) = r_m^2 - \xi^2$  [26][27]. Note that all parameters with units of length are normalized to the background plasma skin depth  $c/\omega_p$ , where  $\omega_p$  is the background plasma frequency. Using the constant of motion given above, the relative longitudinal position of the injected electron can be expressed as

$$\xi \approx \sqrt{4 + \xi_i^2 + r_i^2 - r^2 - 4[\gamma - (v_\phi/c)p_z]} \quad (1)$$

where subscript ‘i’ refers to the position when the electrons are ionized. The electron conducts betatron os-

cillations in  $x$  and  $y$  with a decreasing amplitude under the focusing and acceleration fields [16][28]. An initial isolated slice in  $(\xi_i, x_i, y_i)$  will be mapped to an isolated slice in  $(\xi, x, y, p_z)$  space. If  $r_i \ll 1$  and the transverse momentum (the vector potential of the laser at the time of ionization) are small, the electrons are relativistic and  $p_z/\gamma_\phi^2 \ll 2$  (i.e.,  $\gamma - (v_\phi/c)p_z \ll 1$ ), the position  $\xi$  is mainly determined by the initial  $\xi_i$  as  $\xi \approx \sqrt{4 + \xi_i^2}$ , which means the initial modulation in  $\xi_i$  can be non-linearly mapped to  $\xi$ . This means that an initial slice will be mapped to the same final slice.

Any spread in  $r_i$ ,  $r$  and  $\gamma - (v_\phi/c)p_z$  will broaden the  $\xi$  distribution for an initial slice. In Fig. 1(c) we show the  $(\xi, p_z)$  space at  $z = 0.5\text{mm}$  for an initial slice [indicated by the dashed box in Fig. 1(b)]. One can see that the spread of  $\xi$  due to the spread of transverse motion is  $\Delta\xi_\perp \approx 0.05$ . For this example where a laser driver with moderate  $a_0$  is used, we find that,  $1 - v_\phi/c \approx \omega_p^2/(2\omega_0^2)$  [29]. Therefore, the term  $\gamma - (v_\phi/c)p_z \approx \gamma(1 - v_\phi/c) \approx \omega_p^2/(2\omega_0^2)\gamma$  contributes differently for electrons with different energy leading to a spread in  $\xi$  for electrons with the same  $\xi_i$ . Specifically, electrons ionized earlier (at different  $z_i$ ) but at the same  $\xi_i$  can have higher energy and smaller  $\xi$ . In Fig. 1(c) the difference in  $\xi$  due to the energy difference is seen to be  $\Delta\xi_\gamma \approx 0.1$ . This spread depends on the spread in  $z_i$  which can be controlled by limiting the distance of ionization,  $L_{inj}$ . In the simulations we increased  $L_{inj}$  from  $90\mu\text{m}$  to  $190\mu\text{m}$ , by varying the region where  $\text{N}^{5+}$  existed. In Figs. 1(d)-(f) it can be seen that the difference of  $\xi$  due to this spread in energy is increased to  $\Delta\xi_\gamma \approx 0.2$ . The current profile and the bunching factor (defined as  $b(k) = |\int dz g(z) \exp(ikz)|$ , where  $g(z)$  is the normalized distribution of the trapped electrons) are shown in Fig. 1(d). The modulation in the current profile is peaked at  $k \approx 4k_0$ , and the modulation and the bunching factor are reduced when  $L_{inj}$  is increased from  $90\mu\text{m}$  to  $190\mu\text{m}$  due to the larger  $\Delta\xi_\gamma$ . The discretized phase space structure can be seen clearly in  $(z, x, p_z)$  phase space at  $z = 0.5\text{mm}$  as shown in Figs. 1(e) and (f), however, for the larger  $L_{inj}$ , the slices are slanted in  $(p_z, z)$  space indicating that within a narrow energy slice of the beam the bunching factor can still be large.

By using two pulses to separate the wake formation and the electron injection, the initial and final phase space of the trapped electrons can be better controlled [10, 11, 13–16]. Throughout the rest of this Letter, we consider the driver pulse to be a relativistic electron bunch and the injection pulse to be a co-propagating low intensity laser pulse. The injection laser can be focused to a very small spot size to decrease the transverse ionization region and due to its shorter Rayleigh length it will have a shorter  $L_{inj}$ . This leads to much reduced  $\Delta\xi_\perp$  and  $\Delta\xi_\gamma$ . In a relativistic beam driver case, the phase velocity of the non-linear wake is equal to the velocity of the driver bunch,

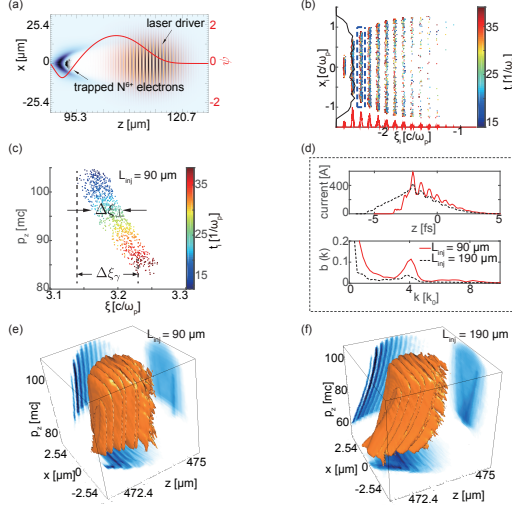


FIG. 1: The nano-scale bunching of injected charge in a PWFA. The laser is focused at  $z = 0\text{mm}$  plane. (a) Snapshot of the charge density distribution of the background electrons, the K-shell electrons of nitrogen, and the laser electric field in  $x$  direction. The red line is the on-axis pseudo potential  $\psi$ . (b) The distribution of the ionization injected electrons in  $(\xi_i, x_i)$  space. The color represents the time when the electrons are ionized. The red peaks are integrated injected charge in  $x_i$  whereas the black is the integrated injected charge for all  $\xi_i$ . (c) The  $(\xi, p_z)$  space at  $z = 0.5\text{mm}$  for an initial slice indicated by the dashed box in (b). (d) The current profile and the bunching factor at  $z = 0.5\text{mm}$ . (e) and (f) show the  $(z, x, p_z)$  phase space at  $z = 0.5\text{mm}$ . For  $L_{inj} = 90\mu\text{m}$  case, the  $\text{N}^{5+}$  ions are distributed from  $z = 0.038\text{mm}$  to  $0.128\text{mm}$  and  $n_{\text{N}^{5+}} = 10^{-3}n_p$ ; for  $L_{inj} = 190\mu\text{m}$  case, the  $\text{N}^{5+}$  ions are distributed from  $z = 0.038\text{mm}$  to  $0.228\text{mm}$  and  $n_{\text{N}^{5+}} = 5 \times 10^{-4}n_p$ .

which is typically closer to the speed of light than the group velocity of the laser. Therefore the term  $\Delta\xi_\gamma$  is much reduced. The electron is longitudinally frozen in the wake after it is boosted to relativistic energy. This longitudinal position can therefore be defined as  $\xi_f$  and this is insensitive when it was ionized.

Under the assumption of no phase slippage in the wake, the effect of the nonlinear mapping between  $\xi_i$  and  $\xi_f$  and the finite  $r_i$  on the bunching factor can be quantified as follows. The distribution of the final longitudinal parameters  $\xi_f$  is  $g(\xi_f)d\xi_f = d\xi_i \int dr_i f(r_i, \xi_i)$  can be obtained from the distribution of the initial parameters is  $f(\xi_i, r_i)$ , where  $r_f$  is neglected which is reasonable when the energy of the electron is high. The bunching factor is  $b(k) = |\int d\xi_i dr_i \exp(ik\xi_f) f(\xi_i, r_i)|$ . Assuming  $\delta\xi_i \equiv \xi_i - \bar{\xi}_i \ll \bar{\xi}_i$  and  $r_i \ll \bar{\xi}_i$  where  $\bar{\xi}_i$  is the mean value of  $\xi_i$ , then after expanding  $\xi_f$  to the order of  $O(r_i^2)$  and  $O(\delta\xi_i^2)$ ,  $\xi_f$  can be expressed as  $\xi_f \approx \sqrt{4 + \bar{\xi}_i^2} \left[ 1 + \frac{\delta\xi_i}{h_m^2 \bar{\xi}_i} + \frac{\delta\xi_i^2}{2h_m^2 \bar{\xi}_i^2} \left( 1 - \frac{1}{h_m^2} \right) + \frac{r_i^2}{2h_m^2 \bar{\xi}_i^2} \right]$ , where  $h_m = \sqrt{4 + \bar{\xi}_i^2}/\bar{\xi}_i$  is the wavenumber upshift factor obtained from the nonlinear mapping process. We assume the initial distribution is  $f(\xi_i, r_i) = \frac{r_i}{\sigma_r^2} \exp\left(-\frac{r_i^2}{2\sigma_r^2}\right) \frac{1}{\sqrt{2\pi}\sigma_e} \exp\left(-\frac{\delta\xi_i^2}{2\sigma_e^2}\right) \sum_{n=-\infty}^{+\infty} F_n \exp(-i2nk_0\delta\xi_i)$ , where  $F_n = \int d\xi_i f_b(\xi_i) \exp(i2nk_0\delta\xi_i)$  and  $f_b(\xi_i)$  is the initial  $\xi_i$  distribution in a single slice. Substitute the expression of  $f(\xi_i, r_i)$  into the bunching factor, then it is straightforward to obtain

$$b(k) = \sum_{n=-\infty}^{+\infty} |F_n| R(\hat{\sigma}_r, \hat{\sigma}_e) e^{-\frac{(k-2nh_mk_0)^2 \sigma_e^2}{2h_m^2(1+\hat{\sigma}_e^4)}} \quad (2)$$

where  $R(\hat{\sigma}_r, \hat{\sigma}_e) = [(1 + \hat{\sigma}_r^4)(1 + \hat{\sigma}_e^4)]^{-1/4}$  is the 3D reduction factor,  $\hat{\sigma}_e = \sigma_e \sqrt{(1 - 1/h_m^2)k/(h_m \bar{\xi}_i)}$  and  $\hat{\sigma}_r = \sigma_r \sqrt{k/(h_m \bar{\xi}_i)}$ . The ratio of the strongest modulation

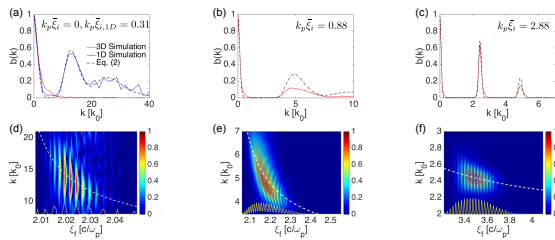


FIG. 2: Bunching of electrons when charges is injected by using a relatively low intensity laser pulse in prescribed and non evolving wakefield. (a), (b) and (c) The red lines are the bunching factor while scanning the initial  $\xi_i$  and the dashed lines are the analytical results from Eq. 2. (d), (e) and (f) The corresponding Wigner transform of the current profile showing the spatial modulation. The white dashed lines are  $k/k_0 = 2\sqrt{4 + \bar{\xi}_i^2}/\bar{\xi}_i$  and the yellow lines are the current profile of the injected charge. Note that (d) is 1D simulation and others are 3D simulations.

wavenumber in the current profile over the wavenumber of the injection laser (the modulation factor) is

$$h = 2h_m = 2\sqrt{4 + \bar{\xi}_i^2}/|\bar{\xi}_i| \quad (3)$$

where the factor 2 is from the ionization process and the factor  $h_m$  is from the nonlinear mapping process. Eq. (3) shows that the wavelength of the modulation is shortest for  $\bar{\xi}_i$  near zero. However,  $\hat{\sigma}_r$  becomes very large for  $\bar{\xi}_i$  near zero, therefore  $R$  will be small in this limit. For this reason the wave number of the modulation is limited and the modulation is only seen when ionization occurs off the maximum of the potential.

These conclusions are verified numerically. We use OSIRIS with non-evolving forces from the nonlinear wakefields, i.e.,  $F_z = -\xi/2, F_r = r/2 + (1 - v_z)r/2$  so no background plasma electrons are needed. An 800 nm laser with  $a_0 = 0.12, w_0 = 2\mu\text{m}$  propagates through a plasma with  $n_p = 1.74 \times 10^{17} \text{cm}^{-3}$  and a  $10^{-5}n_p$   $\text{He}^{1+}$  plasma (to minimize space charge effects) provides the self-trapped electrons via laser ionization. The longitudinal delay between the laser pulse and the plane with  $\xi = 0$  is scanned to generate electrons with different  $\xi_i$  and the resulting bunching factors are shown in Figs. 2(a)-(c). When the laser is strongly focused,  $\gamma - p_z - \psi$  is not strictly conserved and the variation leads to a reduction of the bunching factor which more serious when  $h$  is larger [see Fig. 2(b)]. Due to the nonlinear mapping process, the modulation factor depends on  $\xi_f$ , which can be seen from the Wigner transform of the current profile

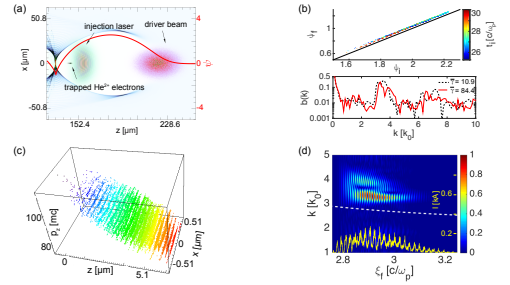


FIG. 3: An electron driver-beam followed by an injection laser propagate to the right in a mixture of pre-ionized plasma and  $\text{He}^{1+}$  ions ( $n_p = 1.74 \times 10^{17} \text{cm}^{-3}, n_{\text{He}^{1+}} = 0.1n_p$ ). Driver-beam:  $E_b = 1\text{GeV}, \sigma_r = 8.9\mu\text{m}, \sigma_z = 10.6\mu\text{m}, I_b = 19\text{kA}$ ; The injection laser is as same as in the case of Fig. 2. (a). Snapshot of the charge density distribution of the background electrons, the 2nd electron of helium, and the laser electric field. The red line is the pseudo potential at the center. (b) The dependence of the final  $\psi_f$  on the initial  $\psi_i$  for injected electrons and the bunching factor at  $z = 0.1\text{mm}$  and  $z = 0.9\text{mm}$ . The color represents the ionization time. The black line represents  $\psi_f = \psi_i - 1$ . (c) The  $(z, x, p_z)$  phase space distribution of the trapped electrons at  $z = 0.9\text{mm}$ . The color represents the  $z$  position. (d) The current (yellow line) and the corresponding Wigner transform at  $z = 0.9\text{mm}$ . The white line is  $k/k_0 = 2\sqrt{4 + \bar{\xi}_i^2}/\bar{\xi}_i$ .

as shown in Figs. 2(d)-(e). The modulation factor can be very high theoretically when  $\xi_i$  is very close to zero, but in this case  $R$  is very small so  $b$  is rather small. However in a 1D simulation,  $h$  as high as 15 was observed as shown in Fig. 2 (d). In each simulation the energy of the electrons is more than 100 MeV.

To verify that nano-bunching exists at high energies including evolving wakes during trapping and acceleration, we next present results from a fully self-consistent 3D OSIRIS simulation. We use a relativistic electron beam to produce the wake for the ionization of the inner shell electrons. A mixture of preionized plasma and  $\text{He}^{1+}$  ions is used. The electric field of the electron beam is low enough to not doubly ionize the He. The simulation window has a dimension of  $127 \times 127 \times 127 \mu\text{m}$  with  $1000 \times 1000 \times 5000$  cells in the  $x, y$  and  $z$  directions, respectively. An injection laser with the same parameters used above (Fig. 2) is focused into the wake as shown in Fig. 3(a). The laser is focused at  $z = 0\text{mm}$  while the plasma starts from  $z = -0.254\text{mm}$ . By tracking particles, we confirm that the trapping condition [4]  $\psi_f \approx \psi_i - 1$  as shown in Fig. 3(b). In Fig. 3(c) we present the phase space distribution of the trapped charge after  $z = 0.9\text{mm}$  for a case where the relative longitudinal position between the beam driver and the injection laser is chosen to achieve  $\xi_i \approx 1.87$ . For this case, based on Eq. 3 the predicted modulator factor is  $h \approx 2.9$ . The bunching factor  $b(k)$  is shown in Fig. 3(b) which is stable when the beam is accelerated from 5.6 MeV to 43.2 MeV. The current profile and the corresponding Wigner transform of the injected charge are shown in Fig. 3(d). The white line  $k/k_0 = 2\sqrt{4 + \xi_i^2}/\xi_i$  does not follow within the center of the Wigner transform because the rear of the wake deviates from a sphere [26][27].

By replacing the 800nm injection laser by its 4th harmonic - 200nm injection laser, an electron bunch with a strong UV frequency modulation is generated. We simulate this using OSIRIS with the external wakefield model described above for the same plasma density. A 200nm injection laser with  $a_0 = 0.023, w_0 = 2\mu\text{m}$  are used to release the 2nd electron of He. The current profile and the bunching factor at  $z = 1.4\text{mm}$  are shown in Fig. 4 respectively where it is seen that individual electrons are

micro bunched spatially on a nano-scale. Such a nano-bunched structure will give rise to intense CTR [21] at the harmonics of the bunching frequency. The CTR energy generated from a sharp plasma-vacuum boundary generated by the modulation within the shaded wave number (frequency) shown in Fig. 4(b) is about 0.02nJ [30] (we assume the beam has a mean energy  $\bar{\gamma} = 1000$ ). The radiated spectrum will contain the fundamental and the second harmonic of the nano-structured beam at 65.6nm and 32.8nm respectively. Detection of this coherent radiation at wavelengths shorter than the ionizing laser wavelength is a good diagnostic of this self-bunching in the wake. Space charge interaction between the injected electrons will blur the modulation at  $nhk_0$  and thus reduce the modulation and the bunching factor at  $nhk_0$  which can be seen from the comparison between the dashed line ( $n_{\text{He}^{1+}} = 3 \times 10^{-5} n_p$ ) and the solid line ( $n_{\text{He}^{1+}} = 0.3 n_p$ ) in Fig. 4(b). Velocity dispersion induced by the energy spread inside a single bunch may destroy nano-bunching at low beam energies. For the results shown in Figs. 2-4, the energy of the beam is sufficient to ensure that velocity dispersion is not an issue if the beam is further accelerated the wake.

Due to the small spot size and low intensity of the injection laser, the emittance and energy spread of the trapped beam are both very small, e.g, for the 200nm injection laser case discussed above  $\epsilon_{nx,y} = 11\text{nm}$ , and uncorrelated energy spread  $\sigma_\gamma = 4$ . If such an electron beam can be accelerated further while limiting the energy spread, extracted from the plasma and coupled into a resonant undulator without degrading its emittance [31] it will produce intense coherent radiation. For example, consider an electron beam with  $\bar{\gamma} = 1068.9$  and  $\sigma_\gamma = 4$  propagating into a planar undulator with wavelength  $\lambda_u = 3\text{cm}$  and normalized undulator parameter  $K = 2$ , which is resonant at the modulation wavelength of the beam,  $\lambda_r = 65.6\text{nm}$ . The output radiation power saturates at  $P_{\text{sat}} = 140\text{MW}$  in 3.5 m undulator when by simulating this process with GENESIS 1.3 code [32]. As a comparison, another FEL simulation using the same beam parameters except with no initial bunching shows that the radiation power achieves 1.1 MW in 9 m undulator.

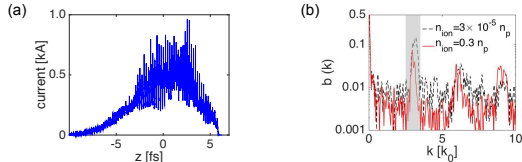


FIG. 4: The current profile (a) and bunching factor (b) of the trapped electrons by using 200nm injection laser at  $z = 1.4\text{mm}$ . The red line is the result when  $n_{\text{He}^{1+}} = 0.3 n_p$  and the black dashed line is the result when  $n_{\text{He}^{1+}} = 3 \times 10^{-5} n_p$ . The energy of the electrons is 50 MeV.

Work supported by the National Basic Research Program of China Grant No. 2013CBA01501, NSFC grants 11425521, 11535006, 11175102, 11005063, thousand young talents program, DOE grants DE-SC0010064, DE-SC0008491, DE-SC0008316, and NSF grants ACI-1339893, PHY-1415386, PHY-0960344. Simulations are performed on the UCLA Hoffman 2 and Dawson 2 Clusters, and the resources of the National Energy Research Scientific Computing Center and the Blue Waters.

---

\* weilu@tsinghua.edu.cn

- [1] C. Joshi and T. Katsouleas, *Physics Today* **56**, 47 (2003).
- [2] M. Chen, Z.-M. Sheng, Y.-Y. Ma, and J. Zhang, *Journal of applied physics* **99**, 056109 (2006).
- [3] E. Oz, S. Deng, T. Katsouleas, P. Muggli, C. D. Barnes, I. Blumenfeld, F. J. Decker, P. Emma, M. J. Hogan, R. Ischebeck, et al., *Phys. Rev. Lett.* **98**, 084801 (2007).
- [4] A. Pak, K. A. Marsh, S. F. Martins, W. Lu, W. B. Mori, and C. Joshi, *Phys. Rev. Lett.* **104**, 025003 (2010).
- [5] C. McGuffey, A. G. R. Thomas, W. Schumaker, T. Matsuoka, V. Chvykov, F. J. Dollar, G. Kalintchenko, V. Yanovsky, A. Maksimchuk, K. Krushelnick, et al., *Phys. Rev. Lett.* **104**, 025004 (2010).
- [6] C. E. Clayton, J. E. Ralph, F. Albert, R. A. Fonseca, S. H. Glenzer, C. Joshi, W. Lu, K. A. Marsh, S. F. Martins, W. B. Mori, et al., *Phys. Rev. Lett.* **105**, 105003 (2010).
- [7] J. S. Liu, C. Q. Xia, W. T. Wang, H. Y. Lu, C. Wang, A. H. Deng, W. T. Li, H. Zhang, X. Y. Liang, Y. X. Leng, et al., *Phys. Rev. Lett.* **107**, 035001 (2011).
- [8] B. B. Pollock, C. E. Clayton, J. E. Ralph, F. Albert, A. Davidson, L. Divol, C. Filip, S. H. Glenzer, K. Herpoldt, W. Lu, et al., *Phys. Rev. Lett.* **107**, 045001 (2011).
- [9] N. Vafaei-Najafabadi, K. A. Marsh, C. E. Clayton, W. An, W. B. Mori, C. Joshi, W. Lu, E. Adli, S. Corde, M. Litos, et al., *Phys. Rev. Lett.* **112**, 025001 (2014).
- [10] B. Hidding, G. Pretzler, J. B. Rosenzweig, T. Königstein, D. Schiller, and D. L. Bruhwiler, *Phys. Rev. Lett.* **108**, 035001 (2012).
- [11] F. Li, J. F. Hua, X. L. Xu, C. J. Zhang, L. X. Yan, Y. C. Du, W. H. Huang, H. B. Chen, C. X. Tang, W. Lu, et al., *Phys. Rev. Lett.* **111**, 015003 (2013).
- [12] N. Bourgeois, J. Cowley, and S. M. Hooker, *Phys. Rev. Lett.* **111**, 155004 (2013).
- [13] A. Martinez de la Ossa, J. Grebenyuk, T. Mehrling, L. Schaper, and J. Osterhoff, *Phys. Rev. Lett.* **111**, 245003 (2013).
- [14] L.-L. Yu, E. Esarey, C. B. Schroeder, J.-L. Vay, C. Benedetti, C. G. R. Geddes, M. Chen, and W. P. Leemans, *Phys. Rev. Lett.* **112**, 125001 (2014).
- [15] X. L. Xu, Y. P. Wu, C. J. Zhang, F. Li, Y. Wan, J. F. Hua, C.-H. Pai, W. Lu, P. Yu, C. Joshi, et al., *Phys. Rev. ST Accel. Beams* **17**, 061301 (2014).
- [16] X. L. Xu, J. F. Hua, F. Li, C. J. Zhang, L. X. Yan, Y. C. Du, W. H. Huang, H. B. Chen, C. X. Tang, W. Lu, et al., *Phys. Rev. Lett.* **112**, 035003 (2014).
- [17] W. P. Leemans, C. E. Clayton, W. B. Mori, K. A. Marsh, A. Dyson, and C. Joshi, *Phys. Rev. Lett.* **68**, 321 (1992).
- [18] W. P. Leemans, C. E. Clayton, W. B. Mori, K. A. Marsh, P. K. Kaw, A. Dyson, C. Joshi, and J. M. Wallace, *Phys. Rev. A* **46**, 1091 (1992).
- [19] A. Lifschitz and V. Malka, *New Journal of Physics* **14**, 053045 (2012).
- [20] M. Zeng, M. Chen, L. L. Yu, W. B. Mori, Z. M. Sheng, B. Hidding, D. A. Jaroszynski, and J. Zhang, *Phys. Rev. Lett.* **114**, 084801 (2015).
- [21] W. Leemans, C. Geddes, J. Faure, C. Tóth, J. Van Tilborg, C. Schroeder, E. Esarey, G. Fubiani, D. Auerbach, B. Marcellis, et al., *Physical review letters* **91**, 074802 (2003).
- [22] R. Fonseca et al., *Lecture notes in computer science* **2331**, 342 (2002).
- [23] C. D. Decker and W. B. Mori, *Phys. Rev. Lett.* **72**, 490 (1994).
- [24] M. V. Ammosov, N. B. Delone, and V. P. Krainov, *Sov. Phys. JETP* **64**, 1191 (1986).
- [25] P. Mora and T. M. Antonsen Jr, *Physics of Plasmas* (1994-present) **4**, 217 (1997).
- [26] W. Lu, C. Huang, M. Zhou, W. B. Mori, and T. Katsouleas, *Phys. Rev. Lett.* **96**, 165002 (2006).
- [27] W. Lu et al., *Phys. Plasma* **13**, 056709 (2006).
- [28] S. Wang, C. E. Clayton, B. E. Blue, E. S. Dodd, K. A. Marsh, W. B. Mori, C. Joshi, S. Lee, P. Muggli, T. Katsouleas, et al., *Phys. Rev. Lett.* **88**, 135004 (2002).
- [29] W. B. Mori, *IEEE J. Quantum Electron.* **33**, 1942 (1997), and references therein.
- [30] L. D. Landau, J. Bell, M. Kearsley, L. Pitaevskii, E. Lifshitz, and J. Sykes, *Electrodynamics of continuous media*, vol. 8 (elsevier, 1984).
- [31] X. L. Xu, J. F. Hua, Y. P. Wu, C. J. Zhang, F. Li, Y. Wan, C.-H. Pai, W. Lu, W. An, P. Yu, et al., *Phys. Rev. Lett.* **116**, 124801 (2016).
- [32] S. Reiche, *Nuclear Instruments and Methods in Physics Research Section A: Accelerators, Spectrometers, Detectors and Associated Equipment* **429**, 243 (1999).